J. Am. Soc. Mass Spectrom. (2011) 22:2145–2159
DOI: 10.1007/s13361-011-0250-5

RESEARCH ARTICLE

Assessment of the Molecular Expression and Structure of Gangliosides in Brain Metastasis of Lung Adenocarcinoma by an Advanced Approach Based on Fully Automated Chip-Nanoelectrospray Mass Spectrometry

Alina D. Zamfir,[1,2] Alina Serb,[3] Željka Vukelić,[4] Corina Flangea,[1,2] Catalin Schiopu,[2] Dragana Fabris,[4] Svjetlana Kalanj-Bognar,[4] Florina Capitan,[3] Eugen Sisu[3,5]

[1]Department of Chemical and Biological Sciences, Aurel Vlaicu University of Arad, Revolutiei Blvd. 77, RO-310130, Arad, Romania
[2]Mass Spectrometry Laboratory, National Institute for Research and Development in Electrochemistry and Condensed Matter, Timisoara, Romania
[3]Victor Babes University of Medicine and Pharmacy, Eftimie Murgu Sq. 2, Timisoara, Romania
[4]Department of Chemistry and Biochemistry, Faculty of Medicine, University of Zagreb, Zagreb, Croatia
[5]Chemistry Institute of the Romanian Academy, Timisoara, Romania

Abstract

Gangliosides (GGs), sialic acid-containing glycosphingolipids, are known to be involved in the invasive/metastatic behavior of brain tumor cells. Development of modern methods for determination of the variations in GG expression and structure during neoplastic cell transformation is a priority in the field of biomedical analysis. In this context, we report here on the first optimization and application of chip-based nanoelectrospray (NanoMate robot) mass spectrometry (MS) for the investigation of gangliosides in a secondary brain tumor. In our work a native GG mixture extracted and purified from brain metastasis of lung adenocarcinoma was screened by NanoMate robot coupled to a quadrupole time-of-flight MS. A native GG mixture from an age-matched healthy brain tissue, sampled and analyzed under identical conditions, served as a control. Comparative MS analysis demonstrated an evident dissimilarity in GG expression in the two tissue types. Brain metastasis is characterized by many species having a reduced *N*-acetylneuraminic acid (Neu5Ac) content, however, modified by fucosylation or *O*-acetylation such as Fuc-GM4, Fuc-GM3, di-*O*-Ac-GM1, *O*-Ac-GM3. In contrast, healthy brain tissue is dominated by longer structures exhibiting from mono- to hexasialylated sugar chains. Also, significant differences in ceramide composition were discovered. By tandem MS using collision-induced dissociation at low energies, brain metastasis-associated GD3 (d18:1/18:0) species as well as an uncommon Fuc-GM1 (d18:1/18:0) detected in the normal brain tissue could be structurally characterized. The novel protocol was able to provide a reliable compositional and structural characterization with high analysis pace and at a sensitivity situated in the fmol range.

Keywords: Quadrupole time-of-flight tandem mass spectrometry, Chip-nanoelectrospray, Gangliosides, Lung adenocarcinoma, Brain metastasis

Correspondence to: Alina D. Zamfir; *e-mail:* alina.zamfir@uav.ro,
Eugen Sisu; *e-mail:* sisueugen@umft.ro

Received: 24 June 2011
Revised: 12 September 2011
Accepted: 12 September 2011
Published online: 15 October 2011

Introduction

Lung adenocarcinoma is a common histologic form of lung cancer that contains certain distinct malignant tissue architectural, cytological, or molecular features. Non-small-cell lung cancer, the most frequent cause of cancer deaths in many countries, has a high risk of brain metastases that reportedly reaches 44% in brain autopsy [1]. Compared with other primary cancers, where brain spread is usually a later complication, lung cancer develops intracranial metastases relatively early and is often accompanied by neurologic symptoms on initial diagnosis [2–6].

Untreated brain metastases have a median survival of about 4 wk with almost all patients dying from neurological rather than systemic causes [7]. Whole-brain radiation therapy and chemotherapy are currently the standard, unfortunately only palliative, treatments for patients with brain metastases. The outcome for patients with brain metastases is generally poor, with median survival time in the range of 3–6 mo [8, 9].

Essentially all types of malignant cells demonstrate changes in their glycosylation at the cell surface and many glycosyl epitopes represent tumor-associated antigens. When highly expressed, some of those epitopes promote invasion and metastasis and thus can lead to shorter survival rate of patients, while some others suppress tumor progression, leading to higher postoperative survival period [10]. Targeting carbohydrate antigens such as gangliosides expressed on tumor cells represents a challenge for the immunotherapy of cancer since aberrant glycosylation exhibited by tumor cells is considered a factor of their uncontrolled growth, invasiveness, and increased metastatic potential [11, 12].

Gangliosides (GGs) are sialic acid-containing glycosphingolipids (GSL) and consist of two main components: a hydrophobic ceramide unit, which anchors the ganglioside to the plasma membrane and a hydrophilic oligosaccharide chain, to which one or more sialic acid groups (*N*-acetylneuraminic acid, Neu5Ac) are attached. They are present in the outer layer of the plasma membranes of all vertebrate cells and are particularly abundant in the central nervous system, where they account for about 6% of the weight of lipids from the brain and the peripheral nervous system; they are also one of the main constituents of lipid rafts [13, 14]. They are involved in numerous processes such as cell communication, adhesion, growth, and differentiation [15], and play a major role in cell recognition and signaling [16]. Since GGs represent major components of the cell surface glycocalyx and participate in cell–cell and cell–matrix interactions, they are implicated in the invasive/metastatic properties of tumor cells [17, 18]. Marked changes in the content and distribution of GGs occur particularly in association with brain tumor formation. Some of these alterations are intrinsic to the neoplastic tumor cells and others are associated with the invasion of tumor-infiltrating host cells. Therefore, changes in their composition and structure during neoplastic transformation have been studied and demonstrated for more than two decades [19–23].

From all lung cancers, non-small cell lung cancer has been shown to exhibit a higher expression levels of GM3 as well as GM3 synthase (sialyltransferase-I or SAT-I) mRNA with a positive correlation between expression levels of SAT-I mRNA and GM3 in tumor tissues [24]. Additionally, overexpression of GM3 synthase was used to determine the effects of endogenous gangliosides on the metastatic process of 3LL Lewis lung carcinoma cells [25].

Recently, it was shown that metastatic potential of mouse Lewis lung cancer cells is regulated via GM1 by modulating the matrix metalloproteinase-9. Low GM1 expressing cell lines showed increase proliferation, invasion, and metastatic potential [26]. Another ganglioside molecule used in development of novel therapies for small cell lung cancer is fucosyl-GM1, which is specifically expressed in lung cancer cells [27]. Thus, in the last year, a bidomainal fucosyl-GM1 ganglioside-based vaccine for the treatment of small-cell lung cancer was developed [28]. It was also shown that an anti-ganglioside-based cancer vaccine containing 1E10 anti-idiotypic monoclonal antibody induces apoptosis and anti-angiogenic effects in a metastatic lung carcinoma [29].

Classic analytical techniques mostly used in GG analysis include ganglioside isolation and purification from the tissue followed by liquid chromatography and different immunochemical methodologies, which can be performed after the chromatographic separation or in direct tissue analysis [30]. Because of its resolving power, robustness, and easy handling, thin layer chromatography (TLC) has been widely used in GSL analysis for more than 30 years [31]. However, for the complete structural analysis of GSL, more sophisticated and advanced techniques are required. Presently, mass spectrometry (MS), intensively exploited for lipid characterization [32, 33], is considered also one of the most precise and sensitive analytical methods in the detection and structural identification of different ganglioside species [34–41].

MS potential for sensitive, accurate, and highly reproducible analysis of complex native GG mixtures increased dramatically by introduction of chip-based nanoelectrospray (nanoESI) MS in the positive and negative ion mode as well as development of instruments able to perform multistage MS (MS^n) experiments for detailed structural elucidation of single components of biomarker value [38, 39].

In the last few years our group was involved in development of chip-based nanoESI techniques and their application in glycolipid analysis for biomedical purposes. Thus, NanoMate robot coupled to either quadrupole time-of-flight (QTOF) or high capacity ion trap (HCT) mass spectrometer was introduced in GSL research for screening, sequencing, and identification of complex ganglioside mixtures extracted from normal [36–38] and pathologic human brain with a particular focus on primary brain tumors [35, 40]. To continue this systematic mapping of gangliosides in brain tumors, in the present study, for the first time, chip-based nanoESI MS was employed for the investigation of ganglioside expression and structure in secondary brain tumors, i.e., brain metastasis of lung adenocarcinoma. Comparative MS

screening of gangliosides from metastatic versus healthy tissue showed considerable discrepancy in expression, structure, and relative abundances of individual species. Moreover, differences in ceramide structures and alteration of sialylation patterns, reported [42] also as tumor-related changes in human carcinomas were discovered. The data acquired by combining chip-based NanoMate with quadrupole time-of-flight (QTOF) MS and high-performance TLC (HPTLC) has confirmed the applied analytical strategy as a powerful tool for finding metastasis-associated structures, which might serve as potential diagnostic markers or specific targets in antitumoral therapy.

Experimental

Characterization of Brain Metastasis Originated from Lung Adenocarcinoma and of Healthy Brain Tissue

Three years following surgery for lung tumor removal, a male patient (73-y-old) reports neurological symptoms such as sudden occipital headaches, dizziness, nausea, and lack of coordination. By computerized tomography, a hyperdense formation having the estimated dimensions 40×40×20 mm was detected in cerebellar vermis. Neurosurgical removal of the tumor mass and pathohistologic examination of tumor tissue (Department of Neurosurgery, University Hospital, Zagreb, Croatia) revealed glandular and papillary structures lined by anaplastic columnar epithelial cells, many of them showing mitotic activity. These findings confirmed the diagnosis of adenocarcinoma brain metastasis. The sample of normal human cerebellum (male, 79-y-old) was dissected to serve as a control; it was obtained from the Department of Forensic Medicine, School of Medicine, University of Zagreb, Croatia. Tissue samples used for biochemical analysis were weighed and stored at −20ºC after careful removal of blood vessels and necrotic elements.

Ganglioside Extraction and Purification

Ganglioside extraction was performed according to the method of Svennerholm and Fredman [43], as modified by Vukelić et al. [44]. Tissue sample was weighed and homogenized in ice-cold distilled water in order to obtain the 10% homogenate. Lipids were extracted twice using solvent mixture of chloroform: methanol (1:2, by vol.), followed by partition and repartition by adding chloroform, methanol, and water to a final 20 volume ratio 1:1:0.8. Upper phases containing polar glycosphingolipids (GGs) were collected. The crude ganglioside extracts were purified in several steps: precipitation of coextracted protein–salt complexes followed by centrifugation; low-molecular-weight contaminants were removed by gel-filtration on Sephadex G-25 column (Pharmacia, Uppsala, Sweden) and dialysis against water (overnight at 4 °C). After complete extraction and purification, the pure ganglioside extracts were evaporated to complete desiccation and weighed.

HPTLC and Laser Densitometry

Ganglioside mixtures isolated and purified from brain metastasis of lung adenocarcinoma and normal cerebellar brain tissue were analyzed in parallel (Figure 1a and b). Quantitative analysis of total ganglioside concentration was performed according to the modified Svennerholm spectrophotometric method [45, 46]. The absorbances of samples and Neu5Ac used as a standard in a range of known concentrations were determined at 580 nm; the concentrations of GG-bound sialic acids (GG-SA) were expressed as microgram GG-SA per gram of fresh tissue w.w. Qualitative analysis was performed by HPTLC separation of individual ganglioside fractions on glass backed HPTLC-plates (silica gel 60, 0.2 mm, 10×10 cm, Merck, Germany). The plates were developed in a solvent system containing chloroform, methanol, and 0.2 aq. $CaCl_2$ (58:40:9, by volume). After drying, the plate was sprayed with resorcinol reagent and heated for 30–45 min until GG fractions appeared as bluish bands. Finally, HPTLC separated and visualized GG fractions were subjected to laser densitometric scanning (LKB 2202 Laser Ultrascan; LKB, Bromma, Sweden) at 580 nm, as described previously [47], enabling relative quantification of individual GG, expressed as the relative proportion (%) in a sample.

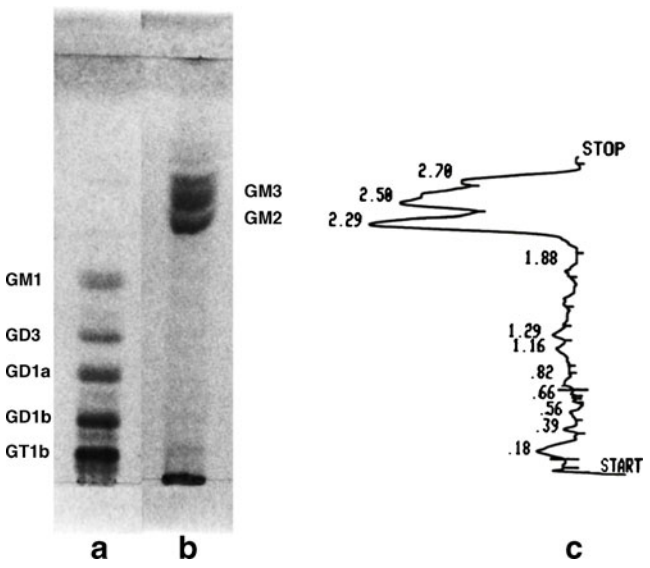

Figure 1. High performance thin-layer chromatography of gangliosides extracted from **(a)** healthy human cerebellar tissue and **(b)** brain metastasis of adenocarcinoma; **(c)** densitometric quantification of ganglioside fractions from brain metastasis of adenocarcinoma

Sample Preparation for MS

For chip-nano ESI MS analysis, the stock solution of each native ganglioside extract (approximately 0.5 mg/mL) was prepared by dissolving the dried material in pure methanol stored at −27 °C. Working aliquots at a concentration of approximately 2.5 pmol/μL (calculated for an average molecular weight of 2000) were obtained by dilution of the stock solution in pure methanol. Methanol was obtained from Merck (Darmstadt, Germany) and used without further purification.

Mass Spectrometry

Mass spectrometry was performed on a QTOF Micromass spectrometer (Waters, Manchester, UK) in the Z-spray geometry. QTOF MS is interfaced to a PC computer running the MassLynx software to control the instrument, acquire, and process MS data. For all acquisitions, the instrument was tuned to record the data at a scan speed of 2.1 scans/s. All mass spectra were acquired in the negative ion mode, since sialylated glycolipids such as GGs exhibit high ionization in negative ion mode. For an efficient ionization and minimal in-source fragmentation, the cone voltage was varied within the range of 40–50 V. For all experiments, the desolvation gas was adjusted within 50 L/h while the ion source temperature was set to 100 °C and kept at this value during the entire experiment. Tandem MS was performed by collision-induced dissociation (CID) at low energies using argon as a collision gas. For ion isolation, the LM and HM parameters were set to 10 and 10, respectively. These values provided a fair compromise between the precursor ion isolation and measurement sensitivity. Collision energy and gas pressure were readjusted several times during the ongoing MS/MS experiment to induce an optimal fragmentation of ganglioside species. The product ion spectra were combined over scans acquired at variable collision energy within a 40–70 eV range (E_{lab}).

All mass spectra were calibrated using as the calibrant a commercially available native mixture of bovine brain gangliosides "Cronassial," from Fidia Research Laboratories (Abano Terme, Italy). The reference provided in negative ion mode a spectrum with a fair ionic coverage of the *m/z* range scanned in both MS and CID MS/MS experiments. The carbohydrate fragment ions were assigned according to the nomenclature introduced by Domon and Costello [48], while the ions corresponding to the fragmentation of the ceramide were designated in agreement with Ann and Adams [49].

Automated Chip-Based Nanoelectrospray

Fully automated chip-nanoESI was performed on a NanoMate 400 robot incorporating ESI chip technology (Advion BioSciences, Ithaca, NY, USA) mounted to the QTOF mass spectrometer. The robot was controlled and manipulated by ChipSoft software operating under Windows system. The position of the electrospray chip was adjusted with respect to the sampling cone potential to give raise to an optimal transfer of the ionic species into the mass spectrometer. In order to prevent any contamination, for all experiments a glass coated microtiter plate was used. Five μL aliquots of the working sample solutions were loaded onto the 96-well plate. The robot was programmed to aspirate the whole volume of sample, followed by 2 μL of air into the pipette tip and then deliver the sample to the inlet side of the microchip. Each nozzle has an internal diameter of 2.5 μm and under the given conditions delivered a flow rate of about 100 nL/min. NanoESI process was initiated by applying voltages within 1.5 to 1.8 kV and a head pressure of 0.5–0.7 p.s.i. After spray initiation, the infusion parameters such as ESI voltage on the pipette tip, cone voltage, and desolvation

Table 1. Proportion of HPTLC-separated ganglioside fractions quantified by densitometric analysis and total ganglioside concentration expressed as total amount of ganglioside-bound sialic acid in (microgram/gram) tissue w.w. in brain metastasis of lung adenocarcinoma

Ganglioside species detected in brain metastasis of lung adenocarcinoma	Proportion of individual gangliosides (laser densitometry, %) in brain metastasis of lung adenocarcinoma tissue	Proportion of individual gangliosides (laser densitometry, %) in healthy cerebellar tissue
GM3	52.27	2.24
GM2	34.81	6.16
GM1	1.26	32.25
GD3	4.97	5.30
GD1a	-	29.76
GD2	1.08	1.73
X1	1.21	Not detected
GD1b	0.77	13.22
GT1b	3.59	7.92
GQ1b	-	0.93
Total concentration of ganglioside-bound sialic acids (μg GG-SA/g tissue)	59.87	817.10
Tumor mass (g)	0.7266	-
Patient's gender and age	male, 73 y	male, 79 y
Primary tumor localization	lungs	-

gas flow were optimized within the specified ranges to enhance a stable spray, proper decomposition of the analyte/solvent clusters, generation of highly charged negative ions, and minimize the in-source fragmentation of labile Neu5Ac or fucose (Fuc) residues. Following sample infusion and MS analysis, the pipette tip was ejected and a fresh tip and nozzle were used for each sample, thus preventing any cross contamination or carry-over.

Results and Discussion

Ganglioside Quantity and Pattern of Brain Metastasis from Lung Adenocarcinoma Analyzed by HPTLC and Laser Densitometry

GGs were extracted and purified from brain metastasis tissue sample weighing 0.7266 g. The total GG content in the sample was 59.87 μg of GG-bound SAs per gram tissue wet weight (w.w.) (μg GG-SA/g), as determined by spectrophotometric method, which is more than 14 times less than the total GG content of healthy adult brain reported by us previously [35]. This corresponds to the lowest total ganglioside content in extraneural tissue, as shown before [50, 51]. Qualitative analysis of GG pattern from brain metastasis sample using HPTLC showed the fractions migrating as GM3, GM2, and less or no visible fraction GT1b, GD1b, GD2, GD3, and GM1 (Figure 1a and b) by simple inspection of the HPTLC plate. Additional minor fraction X1 with TLC migrating properties of monosialo-GG structure was observed only by densitometry scanning (Figure 1c). Proportions of individual GG fractions separated by HPTLC, as quantified by densitometric analysis, differed to a great extent between brain metastasis (Table 1) and healthy brain tissue [35]. In the sample obtained from brain metastasis, the GG fraction with migration properties of GM3 was the major one, accounting for 52.27% of the total GG content followed by GM2 with 34.81%, while proportions of more complex structures (GM1, GD1a, GD1b, and GT1b) were lower compared with healthy brain tissue. The characteristic ganglioside pattern having GM3 and GM2 as the most abundant fractions resembles to ganglioside patterns of normal lung tissue and lung adenocarcinoma, as reported previously [52].

Comparative MS Screening of Ganglioside Mixtures from Healthy and Pathologic Brain Tissue

Purified native ganglioside mixtures extracted from brain metastasis of lung adenocarcinoma located in the cerebellum and from normal cerebellar tissue were submitted to high-throughput (−)nanoESI QTOF MS screening under identical

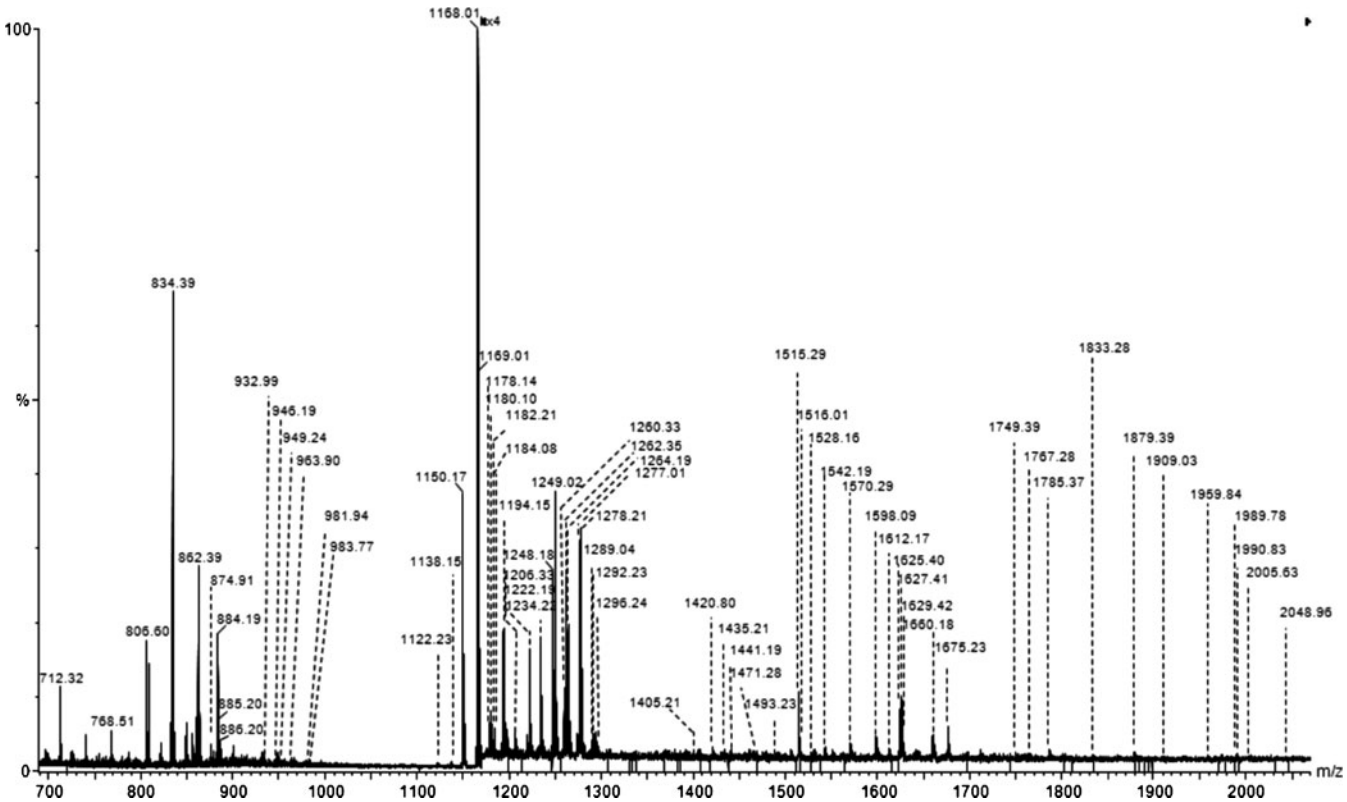

Figure 2. (–)Chip-nanoESI QTOF MS of the native ganglioside mixture isolated from brain metastasis of lung adenocarcinoma. Solvent: MeOH; sample concentration 2.5 pmol/μL; acquisition time 1 min; chip ESI: 1.5 kV; cone voltage: 45 V

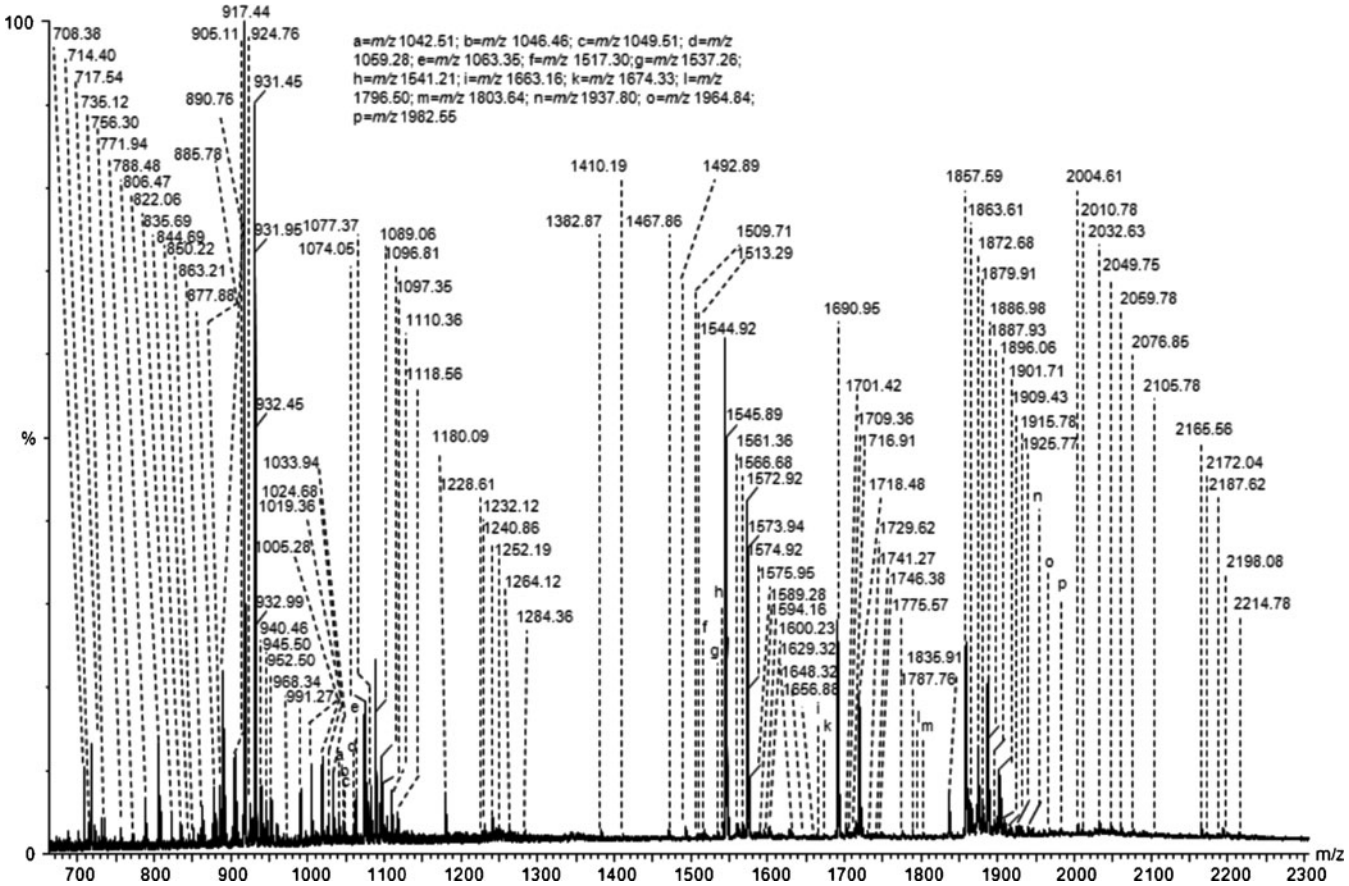

Figure 3. (–)Chip-nanoESI QTOF MS of the native ganglioside mixture isolated from healthy cerebellum tissue. Solvent: MeOH; sample concentration 2.5 pmol/μL; acquisition time 1 min; chip ESI: 1.5 kV; cone voltage: 45 V

solution and instrumental parameters. Each mass spectrum was summed over 20 scans, acquired within only 1 min. Obtained mass spectra are shown in Figures 2 and 3, respectively, while detected GG molecular ions are listed in Tables 2 and 3, together with their putative structural assignment.

The ion assignment and postulation of structures was carried out by mass calculation and was also based on the previously described evidences, knowledge upon this type of substrates [34–41, 53, 54] and known biosynthesis pathway criteria.

While in MS of brain metastasis sample only singly charged ions are present, MS profile of normal cerebellum GG extract is characterized by the presence of singly, doubly, and even triply charged ions. Comparative inspection of the spectra in Figures 2 and 3 obtained under identical experimental conditions highlighted a considerable difference in the number and type of GG components expressed in brain metastasis (Table 2) versus healthy brain tissue (Table 3).

Healthy cerebellar tissue was found to contain a higher variety of GG structures differing in their sialylation degree, from short, monosialylated (GM) to large, polysialylated carbohydrate chains (GH) and also ganglioside chains modified by *O*-acetyl (*O*-Ac) and fucosyl (Fuc) attachments. GM1 (d18:1/18:0) or (d18:0/18:1), GM1 (d18:1/20:0) or (d18:0/20:1) and Fuc-GM1 (18:1/18:0) were detected as abundant singly charged ions at *m/z* 1544.92, 1572.92, and 1690.95 respectively. Beside these species, highly abundant doubly charged ions at *m/z* 917.44 and 931.45 assigned to disialylated GD1 components, with (d18:1/18:0) or (d18:0/18:1) and (d18:1/20:0) or (d18:0/20:1), respectively, were identified as well. Seemingly, healthy brain sample is dominated by mono-, di-, and trisialylated structures. Thus, 28 distinct *m/z* signals correspond to 44 possible GM-type species, 44 *m/z* signals correspond to 63 possible GD- type species, and 32 *m/z* signals are attributable to 59 GT- type species. Most of these structures have a tetrasaccharide sugar core and exhibit high heterogeneity in their ceramide composition. Additionally, six possible tetrasialylated structures (GQ) and only one asialo species (GA) could be detected. Notable is the presence of a hexasialylated GH2 species having (d18:0/24:1) or (d18:1/24:0) Cer constitution. This species was detected as $[M-3H]^{3-}$ at *m/z* 968,34, and was not found in the pathologic brain sample. Eighteen possible GG species modified by fucosylation as well as 30 possible *O*-

Table 2. Ganglioside and asialo-ganglioside species from brain metastasis of lung adenocarcinoma detected by (−)chip-nanoESI QTOF MS analysis of complex native ganglioside mixture

m/z (monoisotopic) theoretical	*m/z* (monoisotopic) experimental	Mass accuracy (ppm)	Molecular ion	Proposed structure
875.19	874.91	33	$[M–H]^-$	LacCer(d18:1/17:0)
933.31	932.99	35	$[M–H]^-$	LacCer(d18:0/21:0)
947.34	947.19	16	$[M–H]^-$	LacCer(d18:0/22:0)
949.22	949.24	21	$[M+2Na–3H]^-$	LacCer(d18:0/19:0)
964.24	963.90	35	$[M–H]^-$	GM4(d18:0/14:0)
982.19	981.94	25	$[M+Na–2H]^-$	GM4(d18:1/14:1)
984.21	983.87	34	$[M+Na–2H]^-$	GM4(d18:1/14:0) or GM4(d18:0/14:1)
1122.48	1122.23	22	$[M–H]^-$	GA2(d18:0/20:0)
1138.44	1138.15	25	$[M–H]^-$	Fuc-GM4(d18:0/16:0)
1138.48		29		GA2(t18:0/20:0)
1150.49	1150.17	28	$[M–H]^-$	GA2(d18:1/21:0)
1150.40		20	$[M–H]^-$	GM3(d18:1/16:1)
1168.42	1168.01	35	$[M–H]^-$	GM3(t18:0/16:0)
1178.46	1178.14	27	$[M–H]^-$	GM3(d18:1/18:1)
1179.74	1180.10	30	$[M–H]^-$	GM3(d18:1/18:0)
1182.49	1182.21	24	$[M–H]^-$	GM3(d18:0/18:0)
1184.37	1184.08	24	$[M–H]^-$	O-Ac-GA1(d18:1/10:0)
1194.50	1194.15	29	$[M–H]^-$	GM3(d18:1/19:0) or GM3(d18:0/19:1)
1206.51	1206.33	15	$[M–H]^-$	GM3(d18:1/20:1)
1206.64		26	$[M–H]^-$	GA2(d18:0/26:0)
1222.51	1222.19	26	$[M–H]^-$	O-Ac-GM3(d18:1/18:0)
1222.55		29	$[M–H]^-$	GM3(d18:0/21:1) or GM3(d18:1/21:0)
1234.56	1234.22	27	$[M–H]^-$	GM3(d18:1/22:1)
1234.52		24		O-Ac-GM3(d18:1/19:1)
1248.55	1248.18	33	$[M–H]^-$	O-Ac-GM3(d18:1/20:1)
1248.59		30		GM3(d18:1/23:1)
1248.59	1249.02	34	$[M–H]^-$	GM3(d18:1/23:0)
1260.60	1260.33	21	$[M–H]^-$	GM3(d18:1/24:2)
1262.62	1262.35	21	$[M–H]^-$	GM3(d18:1/24:1)
1264.63	1264.19	35	$[M–H]^-$	GM3(d18:1/24:0)
1276.61	1277.01	31	$[M–H]^-$	O-Ac-GM3(d18:1/22:0)
1276.64		29	$[M–H]^-$	GM3(d20:1/23:1)
1276.69		25	$[M–H]^-(-H_2O)$	GM3(d18:0/26:0)
1278.66	1278.21	35	$[M–H]^-$	GM3(d20:1/23:0)
1278.61		31	$[M–H]^-$	O-Ac-GM3(d18:1/22:0) or O-Ac-GM3(d18:0/22:1)
1288.67	1289. 04	29	$[M–H]^-$	GM3(d18:1/26:2) or GM3(d18:2/26:1)
1288.67		29	$[M–H]^-$	GM3(d20:1/24:2)
1292.68	1292.23	35	$[M-H]^-$	GM3(d18:1/26:0) or GM3(d18:0/26:1)
1296.54	1296.24	23	$[M–H]^-$	Fuc-GM3(d18:1/16:1)
1296.59		27	$[M–H]^-$	O-Ac-GA1(d18:1/18:0)
1296.61		28	$[M–H]^-$	GA1(d18:0/21:0) or GA1(d18:0/21:0)
1405.65	1405.21	31	$[M+Na–2H]^-$	GM2(d18:1/18:0)
1420.68	1420.80	8	$[M–H]^-$	O-Ac-GM2(d18:2/18:2)
1435.59	1435.21	26	$[M+Na–2H]^-$	GD3(d18:1/14:1) or GD3(d18:0/14:2) or GD3(d18:2/14:0)
1441.66	1441.19	33	$[M–H]^-$	GD3(d18:1/16:1) or GD3(d18:0/16:2) or GD3(d18:2/16:0)
1471.73	1471.28	31	$[M–H]^-$	GD3(d18:1/18:0)
1493.71	1493.23	32	$[M+Na–2H]^-$	GD3(d18:1/18:0)
1515.69	1515.29	26	$[M+2Na–3H]^-$	GD3(d18:1/18:0) or GD3(d18:0/18:1)
1515.74		30	$[M–H]^-$	GM1(d18:1/16:1) or GM1(d18:0/16:2) or GM1(d18:2/16:0)
1515.78		32	$[M–H]^-$	O-Ac-GD3(d18:0/18:0)
1515.71	1516.01	20	$[M+Na–2H]^-$	GD3(d18:1/20:2) or GD3(d18:0/20:3) or GD3(d18:2/20:1)
1515.75		17	$[M–H]^-$	GM1(d18:2/16:0) or GM1(d18:1/16:1) GM1(d18:0/16:2)
1527.83	1528. 16	22	$[M–H]^-$	GD3(d18:0/22:0)
1541.79	1542. 19	26	$[M–H]^-$	GM1(d18:1/18:2) or GM1(d18:2/18:1) or GM1(d18:0/18:3)
1569.78	1570.29	32	$[M+2Na–3H]^-$	GD3(d18:1/22:0) or GD3(d18:0/22:1)
1569.83		29	$[M–H]^-$	GM1(d18:1/20:1) or GM1(d18:0/20:2) or GM1(d18:2/20:0)
1569.77		33	$[M+Na–2H]^-$	GD3(d18:0/24:2) or GD3(d18:1/24:1) or GD3(d18:2/24:0)
1597.88	1598.09	13	$[M–H]^-$	GM1(d18:0/22:2) or GM1(d18:1/22:1) or GM1(d18:2/22:0)
1611.77	1612.17	25	$[M+2Na–3H]^-$	GM1(d18:1/20:2)
1625.89	1625.40	30	$[M+2Na–3H]^-$	GD3(d18:1/26:1) or GD3(d18:0/26:2) or
1624.92		30	$[M–H]^-$	GD3(d18:2/26:0) GM1(d18:1/24:2)
1627.90	1627.41	30	$[M+2Na–3H]^-$	GD3(d18:0/26:1) or GD3(d18:1/26:0)
1626.93		29	$[M–H]^-$	GM1(d18:0/24:2) or GM1(d18:1/24:1) or GM1(d18:2/24:0)
1629.92	1629.42	31	$[M–H]^-$	GM1(d18:0/24:1) or GM1(d18:1/24:0)
1628.94		29	$[M–H]^-$	di-O-Ac-GM1(d18:1/18:0)
1659.79	1660.18	23	$[M+3Na–4H]^-$	GM1(d18:1/22:3) or GM1(d18:0/22:4) or GM1(d18:2/22:2)

Table 2. (continued)

m/z (monoisotopic) theoretical	*m/z* (monoisotopic) experimental	Mass accuracy (ppm)	Molecular ion	Proposed structure
1674.87	1675.23	21	$[M+Na-2H]^-$ ($-H_2O$)	GD2 (d18:1/18:2)
1748.97	1749.39	24	$[M+Na-2H]^-$	GD2 (d18:1/22:1)
1766.97	1767.28	18	$[M-H]^-(-H_2O)$	GT3 (d18:1/20:1)
1785.07	1785.37	17	$[M-H]^-$	O-Ac-GD2(d18:1/23:0) or O-Ac-GD2(d18:0/23:1)
1833.81	1833.28	29	$[M-H]^-$	GT3(d18:0/23:0)
1833.07		11	$[M-H]^-$	O-Ac-GT3 (d18:0/20:0)
1861.12	1861.24	6	$[M-H]^-$	O-Ac-GT3-lactone(d18:0/22:0)
1861.12		6	[M–H] ($-H_2O$)	O-Ac-GT3(d18:0/22:0)
1879.09	1879.39	16	$[M+Na-2H]^-$	O-Ac-GT3 (d18:2/22:1)
1879.10		15	$[M-H]^-(-H_2O)$	Fuc-GT3(d18:0/17:0)
1879.99		32	$[M-H]^-$	GT2(d18:1/12:1) or GT2(d18:2/12:0)
1909.16	1909.03	7	$[M-H]^-$	GD1 (d18:1/22:0)
1960.21	1959.84	19	$[M-H]^-(-2H_2O)$	GT2(d18:0/20:0)
1960.12		14	$[M-H]^-$	GT2(d18:1/18:3) or GT2(d18:2/18:2)
1990.17	1989.78	20	$[M+Na-2H]^-$	GT2(d18:0/18:0)
1990.19		21	$[M-H]^-$	GT2(d18:0/20:3) or GT2(d18:1/20:2) or GT2(d18:2/20:1)
1990.19	1990.83	32	$[M-H]^-$	GT2(d18:1/20:1) or GT2(d18:0/20:2) or GT2(d18:2/20:0)
2005.20	2005.63	21	$[M-H]^-$	Fuc-GD1(d18:1/20:2)
2006.19		28		O-Ac-GT2(d18:1/18:1)
2048.23	2048.80	28	$[M-H]^-$	di-O-Ac-GT2(d18:0/18:0)
2048.10		34	$[M-H]^-(-H_2O)$	GT1(d18:2/14:2) or GT1(d18:3/14:1)

acetylated GG variants were also identified. Most of the fucosylated components are of GM1 and GD1-type with different fatty acid and/or sphingoid base compositions in the Cer moiety. Unlike fucosylation, *O*-acetylation was found for a higher variety of glycoforms such as GM3, GM1, GD3, GD2, GD1, GT3, GT2, GT1, and GQ1, which differ not only in oligosaccharide chain composition but also in their sialylation status. Interestingly, four possible di-*O*-Ac GG variants of GT2, GM1, and GM3 were detected as well.

In contrast to healthy cerebellar tissue, the ganglioside mixture extracted from brain metastasis of lung adenocarcinoma exhibits mostly species of short oligosaccharide chains and reduced overall sialic acid content. More than a half, from the total of 59 different ions detected and corresponding to 125 possible structures in brain metastatic tissue, represent monosialylated species of GM1, GM2, GM3, and GM4-type. Besides the large number of monosialylated components, eight asialo species of GA1 and GA2-type bearing ceramides of variable constitution are present. GD1, GD2, and GD3 as well as GT1, GT2, and GT3 with short carbohydrate chains, expressing different ceramide portions were also identified in the mixture. Ganglioside components modified by Fuc or *O*-Ac could also be detected, but in a different pattern than in healthy cerebellum; most *O*-acetylated gangliosides are monosialo species of GM3, as well as short GT3- and GT2- type, while fucosylated components are represented by monosialo species of GM3 and GM4 structure, di- and trisialylated GD1 and GT3 exhibiting high heterogeneity in their ceramide motifs.

The most abundant singly charged ions at *m/z* 1150.17, 1168.01, 1515.29, and 1627.41 are assigned to GA2 (d18:0/22:0) or GM3 (d18:1/16:1); GM3 (t18:0/16:0); sodiated GD3 (d18:1/18:0) or (d18:0/18:1) or GM1 (d18:1/16:1) or (d18:0/16:2) or GM1 (d18:2/16:0) or *O-Ac*-GD3 (d18:0/18:0) and sodiated GD3 (d18:1/26:0) or (d18:0/26:1) or GM1 (d18:0/24:2) or (d18:1/24:1) or (d18:2/24:0).

CID MS/MS Analysis of GD3 (d18:1/18:0) Species Associated with Brain Metastasis of Lung Adenocarcinoma

To achieve a complete structural characterization of GD3 (d18:1/18:0) species associated with brain metastasis of lung adenocarcinoma, the monodeprotonated species at *m/z* 1471.29 corresponding according to mass calculation to GD3 (d18:1/18:0) was isolated and submitted to fragmentation using CID at low energies. Obtained MS/MS results are presented in Figure 4, together with a scheme depicting the fragmentation pathway experienced by the precursor ions during the dissociation event (inset Figure 4).

As visible, chip-nanoESI MS/MS gave rise to product ions useful for a reliable assignment of the entire carbohydrate sequence of the disialylated species, as well as for characterization of the type of its ceramide portion. Loss of one terminal Neu5Ac is evidenced by the presence of abundant Y_3^- fragment ion at *m/z* 1178.69 accompanied by the corresponding dehydrated Z_3^- form at *m/z* 1160.67 and Y_3^-/CO_2 at *m/z* 1134.62. Subsequent mono-desialylation is documented by the asialo Y_2^- fragment at *m/z* 888.19 and also B_1^- ($Neu5Ac^-$) at *m/z* 290.16, B_2^- ($Neu5Ac_2^-$) at *m/z* 581.24, B_2^-/CO_2 at *m/z* 537.21, $B_2^-/CO_2/H_2O$ at *m/z* 519.20, and C_2^- at *m/z* 599.26.

Cleavage of the ceramide moiety gave rise to the singly charged Y_0^- ion at *m/z* 564.00. This fragment ion along with

Table 3. Ganglioside and asialo-ganglioside species from healthy cerebellum detected by (−)chip-nanoESI QTOF MS analysis of complex native ganglioside mixture

m/z (monoisotopic) theoretical	*m/z* (monoisotopic) experimental	Mass accuracy (ppm)	Molecular ion	Proposed structure
708.35	708.38	4	$[M–3H]^{3–}$	GT1(d18:1/18:0)
714.42	714.40	3	$[M–3H]^{3–}$	GT1(t18:0/18:0)
			$[M+Na–4H]^{3–}$	GT1(d18:1/18:2)
717.58	717.54	5	$[M–3H]^{3–}$	GT1(d18:1/20:0) or GT1(d18:0/20:1)
734.91	735.12	29	$[M–2H]^{2–}$	GD3(d18:1/18:0) or GD3(d18:0/18:1)
756.38	756.30	11	$[M–2H]^{2–}$	O-Ac-GD3(d18:1/18:0)
771.95	771.93	3	$[M–2H]^{2–}$	GM1(d18:0/18:1) or GM1(d18:1/18:0)
822.05	822.06	1	$[M+Na–4H]^{3–}$	GQ1(d18:1/20:0) or GQ1(d18:0/20:1)
835.95	835.69	31	$[M–2H]^{2–}$	GD2(d18:1/18:1) or GD2(d18:0/18:2) or GD2(d18:2/18:0)
844.96	844.69	32	$[M–2H]^{2–}$	O-Ac-GD2(d18:0/16:0)
850.47	850.22	29	$[M–2H]^{2–}$	GD2 (d18:1/20:0)
863.51	863.21	35	$[M–2H]^{2–}$	Fuc-GM1(d18:1/22:2) or Fuc-GM1(d18:0/22:3) or Fuc-GM1(d18:2/22:1)
863.00		24	$[M–2H]^{2–}$	GD2(d18:0/22:3) or GD2(d18:1/22:2) or GD2(d18:2/22:1)
862.99		26	$[M+Na–3H]^{2–}$	GD2(d18:0/20:0)
878.03	877.88	17	$[M–2H]^{2–}$	GD2(d18:1/24:1)
886.03	885.78	28	$[M–2H]^{-}$	O-Ac-GD2(d18:1/22:0) or O-Ac-GD2(d18:0/22:1)
890.97	890.76	24	$[M+Na–3H]^{2–}$	GT3(d18:1/18:1)
905.01	905.11	11	$[M+Na–3H]^{2–}$	GT3(d18:1/20:0)
917.48	917.44	4	$[M–2H]^{2–}$	GD1(d18:1/18:0) or GD1(d18:0/18:1)
924.49	924.76	29	$[M–2H]^{2–}$	GD1(d18:1/19:0) or
924.53		25	$[M+2Na–4H]^{2–}$	O-Ac-GT3(t18:1/20:0) or O-Ac-GT3(d18:0/20:1)
931.49	931.45	4	$[M–2H]^{2–}$	GD1(d18:1/20:0) or GD1(d18:0/20:1)
940.50	940.46	4	$[M–2H]^{2–}$	GD1(t18:0/20:0)
940.19		29	$[M+2Na–4H]^{2–}$	GD1 (d18:1/18:0) or GD1(d18:0/18:1)
945.51	945.50	1	$[M–2H]^{2–}$	GD1(d18:1/22:0)
952.52	952.50	2	$[M–2H]^{2–}$	O-Ac-GD1 (d18:1/20:0) or O-Ac-GD1 (d18:0/20:1)
968.03	968.34	32	$[M–3H]^{3–}$	GH2(d18:1/24:0) or GH2(d18:0/24:1)
991.56	991.27	29	$[M+Na–3H]^{2–}$	GT2(d18:1/18:2) or GT2(d18:0/18:3) or GT2(d18:2/18:3)
1005.58	1005.28	30	$[M+2Na–4H]^{2–}$	GT2 (d18:0/18:0)
1019.02	1019.36	33	$[M–2H]^{2–}$	GalNAc-GD1(d18:0/18:0)
1024.62	1024.68	6	$[M–2H]^{2–}$	di-O-Ac-GT2 (d18:1/18:0)
1024.57		11	$[M+2Na–4H]^{2–}$	O-Ac-GT2 (d18:1/18:1)
1034.24	1033.94	29	$[M+2Na–3H]^{-}$	GM4 (d18:1/16:0) or GM4 (d18:0/16:1)
1042.60	1042.51	9	$[M–2H]^{2}$	GT1 (t18:1/14:1) or
1042.66		14		GalNAc-GD1(t18:0/20:0)
1046.59	1046.46	12	$[M+Na–3H]^{2–}$	GT1(d18:1/14:0) or GT1(d18:0/14:1)
1049.62	1049.51	10	$[M–2H]^{2–}$	GT1(d18:1/16:0) or GT1(d18:0/16:1)
1059.61	1059.28	31	$[M+Na-3H]^{2–}$	GT1(d18:1/16:1)
1063.03	1063.35	30	$[M–2H]^{2–}$	GT1(d18:1/18:0) or GT1(d18:0/18:1)
1074.02	1074.05	3	$[M+Na–3H]^{2–}$	GT1(d18:1/18:0)
1077.04	1077.37	31	$[M–2H]^{2–}$	GT1\(d18:1/20:0)
1097.18	1096.81	34	$M–2H]^{2–}$	O-Ac-GT1(d18:1/20:1) or O-Ac-GT1(d18:0/20:2) or O-Ac-GT1(d18:2/20:0)
1097.04		21	$[M+Na–3H]^{2–}$	GT1(t18:0/20:0)
1110.70	1110.36	31	$[M-2H]^{2–}$	O-Ac-GT1(d18:1/22:2)
1118.49	1118.56	6	$[M–H]^{–}$	GM4(t18:1/24:0)
1180.47	1180.09	32	$[M–H]^{–}$	GM3(d18:1/18:0) or GM3(d18:0/18:1)
1228.51	1228.61	8	$[M–H]^{–}$	GA1(d18:0/16:0)
1228.49		10	$[M+Na–2H]^{–}$	GM3(d18:1/20:1) or GM3(d18:0/20:2)
1232.55	1232.12	35	$[M–H]^{–}$	GM3(d18:1/22:2) or GM3(d18:0/22:3) or GM3(d18:2/22:1)
1232.52		32	$[M+Na–2H]^{–}$	GM3(d18:0/20:0)
1241.29	1240.86	35	$[M+Na–3H]^{2–}$	O-Ac-GQ1(d18:1/18:0)
1252.58	1252.19	31	$[M–H]^{–}$	O-Ac-GM3(d18:0/20:0)
1252.60		33		GM3 (d18:0/23:0)
1264.54	1264.12	33	$[M–H]^{–}$	di-O-Ac-GM3(d18:1/18:0)
1284.60	1284.36	19	$[M+Na–2H]^{–}$	GM3(d18:1/24:1)
1382.82	1382.87	4	$[M–H]^{–}$	GM2(d18:1/18:0) or GM2(d18:0/18:1)
1409.70	1410.19	35	$[M–H]^{–}$	GM2(d18:1/20:0) or GM2(d18:0/20:1)
1467.69	1467.86	12	$[M–H]^{–}$	GD3(d18:1/18:2)
1467.67		13	$[M+Na–2H]^{–}$	GD3(d18:0/16:0)
1492.81	1492.89	5	$[M+Na–2H]^{–}$	GD3(d18:1/18:0)
1509.73	1509.71	1	$[M–H]^{–}$	O-Ac-GD3(d18:1/18:1)
1509.79		5		Fuc-GM2-lactone (d18:1/18:1)

Table 3. (continued)

m/z (monoisotopic) theoretical	*m/z* (monoisotopic) experimental	Mass accuracy (ppm)	Molecular ion	Proposed structure
1513.76	1513.29	31	$[M–H]^-$	O-Ac-GD3(d18:1/18:0)
1516.84	1517.30	30	$[M–H]^-$	GM1(d18:1/16:0) GD3(d18:2/20:2)
1517.71		27	$[M+Na–2H]^-$	Fuc-GM2(d18:2/16:2)
1517.70		26	$[M+Na–2H]^-$	
1537.72	1537.26	30	$[M+Na–2H]^-$	GM1(d18:1/16:1)
1541.73	1541.21	33	$[M+2Na–3H]^-$	GD3(d18:1/20:0)
1544.87	1544.92	3	$[M–H]^-$	GM1(d18:1/18:0) or GM1(d18:0/18:1)
1561.80	1561.36	28	$[M–H]^-$	O-Ac-GM1(d18:0/16:0)
1566.85	1566.68	11	$[M+Na–2H]^-$	GM1(d18:1/18:0) or GM1(d18:0/18:1)
1572.90	1572.92	1	$[M–H]^-$	GM1(d18:1/20:0) or GM1(d18:0/20:1)
1589.83	1589.28	35	$[M–H]^-$	Fuc-GD3(d18:1/16:0)
1593.82	1594.16	21	$[M+Na–2H]^-$	GM1(d18:1/20:0)
1599.89	1600.23	21	$[M–H]^-$	GM1(d18:0/22:0)
1629.88	1629.32	34	$[M–H]^-$	di-O-Ac-GM1(d18:1/18:0)
1648.88	1648.32	34	$[M–H]^-$	GD2(d18:0/16:0)
1656.90	1656.88	1	$[M–H]^-$	GD2-lactone (d18:1/18:0)
1662.82	1663.16	20	$[M+Na–2H]^-$	GD2(d18:2/16:2)
1674.92	1674.33	35	$[M–H]^-$	GD2(d18:1/18:0) or GD2(d18:0/18:1)
1690.93	1690.95	1	$[M–H]^-$	Fuc-GM1(d18:1/18:0)
1700.96	1701.42	27	$[M–H]^-$	GD2(d18:1/20:0) or GD2(d18:0/20:1)
1708.88	1709.36	27	$[M+Na–2H]^-$	O-Ac-GD2 (d18:1/16:1)
1716.94	1716.91	2	$[M–H]^-$	Fuc-GM1 (d18:1/20:1)
1717.98	1718.48	29	$[M–H]^-$	Fuc-GM1 (d18:1/20:0)
1729.01	1729.62	35	$[M–H]^-$	GD2(d18:1/22:0) or GD2(d18:0/22:1)
1741.87	1741.27	34	$[M+Na–2H]^-$	Fuc-GM1 (d18:0/20:0)
1746.92	1746.38	31	$[M+2Na–3H]^-$	GD2(d18:0/20:0)
1775.04	1775.57	30	$[M+Na–2H]^-$	GD2(d18:2/24:3)
1787.98	1787.76	12	$[M+2Na–3H]^-$	Fuc-GM1(d18:1/22:1)
1796.07	1796.50	24	$[M+Na–2H]^-$	Fuc-GM1(d18:1/24:0)
1803.02	1803.64	34	$[M–H]^-$	O-Ac-GT3(d18:1/18:1)
1835.96	1835.91	3	$[M–H]^-$	GD1(d18:1/18:0) or GD1(d18:0/18:1)
1857.02	1857.59	31	$[M+Na–2H]^-$	GD1(d18:0/18:0)
1863.10	1863.61	27	$[M–H]^-$	GD1(d18:1/20:0)
1873.07	1872.68	21	$[M+Na-2H]^-$	GD1(d18:1/19:0)
1879.93	1879.91	1	$[M+2Na–3H]^-$	GD1(d18:1/18:0)
1887.79	1886.98	5	$[M–H]^-$	Fuc-GT3-lactone(d18:1/18:2) Fuc-GT3-lactone(d18:0/18:3) Fuc-GT3-lactone(d18:2/18:1)
1895.96	1896.06	5	$[M+2Na–3H]^-$	GD1(d18:0/19:0)
1901.05	1901.71	35	$[M+2Na–3H]^-$	O-Ac-GT3(d18:1/22:1)
1910.07	1909.43	34	$[M–H]^-$	GT2(d18:0/14:0) or GT2(d18:0/14:1)
1915.17	1915.78	31	$[M–H]^-$	GD1(d18:1/24:2)
1925.14	1925.77	33	$[M+Na–2H]^-$	GD1(d18:1/23:1)
1937.15	1937.80	34	$[M+Na–2H]^-$	GD1(d18:1/24:2) or GD1(d18:0/24:3) or GD1(d18:2/24:1)
1964.16	1964.84	35	$[M–H]^-$	GT2(d18:0/18:0)
1983.20	1982.55	33	$[M–H]^-$	Fuc-GD1(d18:1/18:0)
2005.20	2004.61	30	$[M–H]^-$	Fuc-GD1(d18:1/20:2)
2010.16	2010.78	31	$[M+Na–2H]^-$	GT2(d18:1/20:2) or GT2(d18:0/20:3) or GT2(d18:2/20:1)
2032.23	2032.63	20	$[M–H]^-$	O-Ac-GT2(d18:1/20:1) or O-Ac-GT2(d18:0/20:2) or O-Ac-GT2(d18:2/20:0)
2032.14		24	$[M+2Na–3H]^-$	GT2(d18:1/20:2) or GT2(d18:0/20:3) or GT2(d18:2/20:1)
2050.24	2049.75	24	$[M–H]^-$	di-O-Ac-GT2 (d18:1/18:0)
2059.27	2059.78		$[M+Na–2H]^-$	Fuc-GD1(d18:1/22:0)
2076.24	2076.85	29	$[M–H]^-$	GQ3(d18:1/20:2) or GQ3(d18:0/20:3) or GQ3(d18:2/20:1)
2106.27	2105.78	23	$[M–H]^-$ $(-H_2O)$	GT1(d18:1/18:2)
2166.32	2165.56	35	$[M–H]^-$	O-Ac-GT1(d18:1/18:2) or O-Ac-GT1(d18:0/18:3) or O-Ac-GT1(d18:2/18:1)
2165.03		24	$[M+Na–2H]^-$	GT1(t18:1/18:0) O-Ac-
2166.29		34		GT1(d18:1/16:0)
2172.19	2172.04	7	$[M+2Na–3H]^-$	O-Ac-GT1(t18:1/14:1)
2188.38	2187.62	35	$[M+Na–2H]^-(-H_2O)$	GT1(d18:1/22:0)
2188.39		35	$[M+Na–2H]^-$	GT1(d18:1/21:1)
2198.31	2198.08	10	$[M+2Na–3H]^-$	GT1(d18:1/20:0)
2214.25	2215.78	24	$[M+Na–2H]^-$	O-Ac-GT1(d18:1/20:2)

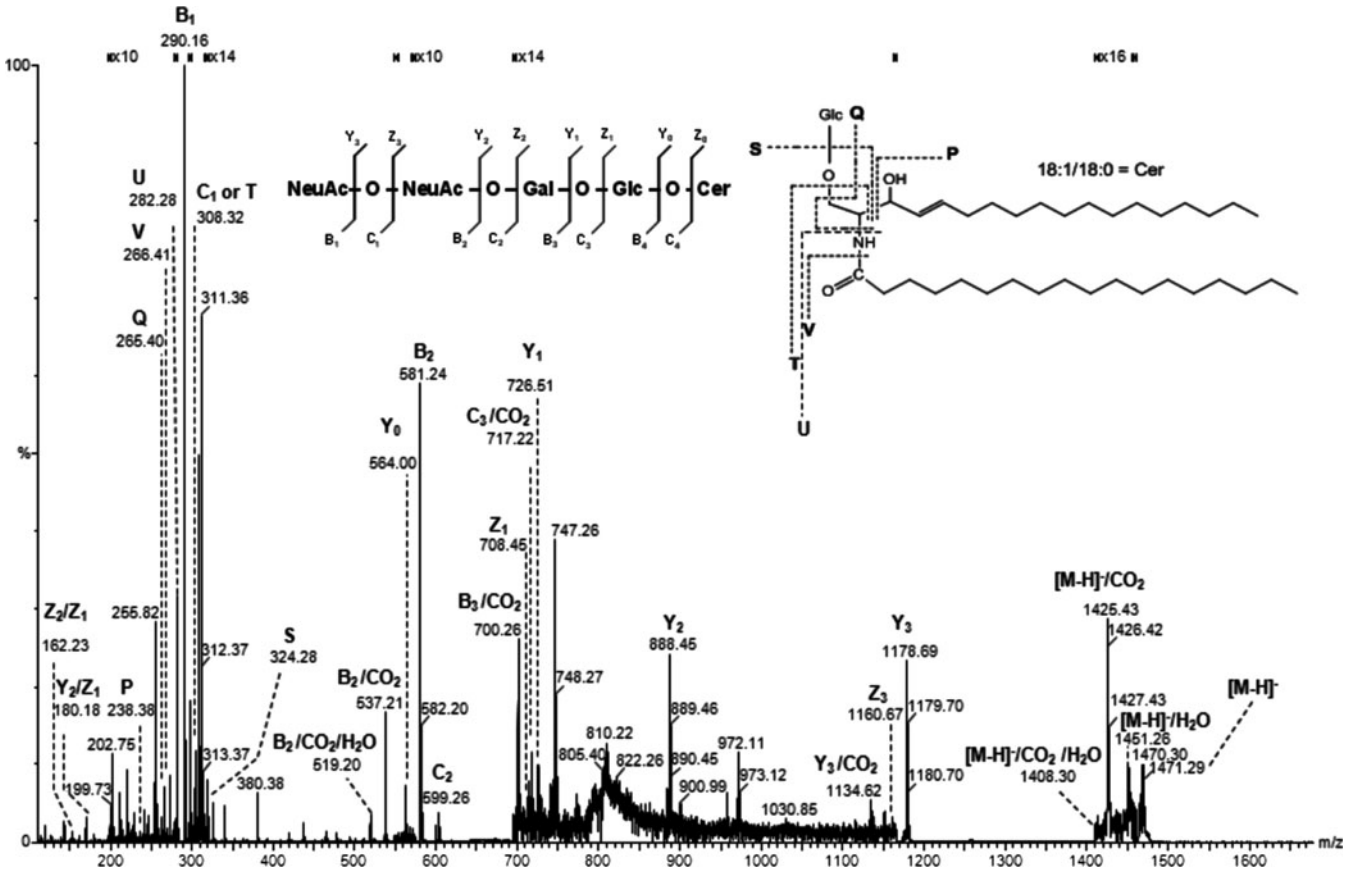

Figure 4. (–)Chip-nanoESI QTOF CID MS/MS of the singly charged ion at *m/z* 1471.29 corresponding to GD3 (d18:1/18:0) from brain metastasis of lung adenocarcinoma. Acquisition time 1 min. Insets: fragmentation schemes of the oligosaccharide core and ceramide moiety

the singly charged ions: Y_1^- at *m/z* 726.51 (GlcCer), its dehydrated counterpart Z_1^- at *m/z* 708.45, Y_2^- at *m/z* 888.45 (GalGlcCer), B_3^-/CO_2 at *m/z* 700.26, and C_3^-/CO_2 at *m/z* 717.22 characterize the carbohydrate sequence and document a (d18:1/18:0) ceramide configuration. This structure of the ceramide is supported also by the Cer-derived fragment ions at *m/z* 238.38, 265.40, 266.41, 282.28, 308.32, and 324.28 attributable to P, Q, V, U, T, and S type of ions, respectively (Figure 4, inset).

CID MS/MS Analysis of Fuc-GM1 (d18:1/18:0) Species from Healthy Brain Tissue

Figure 5 presents QTOF CID MS/MS of the singly charged ion at *m/z* 1690.95, which, according to calculation, corresponds to Fuc-GM1 (d18:1/18:0). To determine the oligosaccharide and ceramide composition as well as for collecting specific data upon Neu5Ac and Fuc residue localization, the MS/MS conditions were optimized to provide as many informative sequence ions as possible. Consequently, spectra in Figure 5 feature a high number of structurally-informative ions. Thus, Y_1^- ion at *m/z* 726.46 and its dehydrated counterpart Z_1^- at *m/z* 708.47, $Y_{2\alpha}^-$ at *m/z* 1325.81, and $Y_{3\alpha}^-$ at *m/z* 1382.97 together with its counterpart $Z_{3\alpha}^-$ at *m/z* 1364.87 obtained after water elimination correspond to Gal-GalNAc-Gal-Glc-Cer$^-$. Inevitably, these abundant ions were found accompanied by product ions derived from the loss of one or both labile attachments of Fuc and Neu5Ac, respectively. However, a comparison with the fragmentation pattern of human brain GM1(d18:1/18:0), obtained previously [53] on a QTOF MS instrument under similar CID conditions, indicates that in the spectrum in Figure 5 a number of ions shifted with Δm =146 u, the mass of Fuc residue, are diagnostic for fucosylation. Fuc attachment site at the inner Gal (as shown in Figure 6) was found well documented by $Y_{3\alpha}^-$ ion at *m/z* 1382.97 and its dehydrated counterpart $Z_{3\alpha}^-$ at *m/z* 1364.87, $Y_{2\alpha}^-$ at *m/z* 1325.81, $Y_{3\alpha}^-/Y_{1\beta}^-$ at *m/z* 1091.80 corresponding to Gal-NAc-Gal(Fuc)-Glc-Cer$^-$ (d18:1/18:0) sequence and $Z_{3\alpha}^-/Y_{1\beta}^-$ complement at *m/z* 1073.77 occurred after water elimination. Fuc attachment to the inner Gal is a result of either α1-2 or α1-6 fucosyltransferase action [55].

Due to the high structural selectivity, a number of fragment ions were found also diagnostics for the localization of Neu5Ac moiety at the inner Gal of the monosialotetraose-Cer (d18:1/18:0) oligosaccharide backbone; these are $Y_{2\alpha}^-$ at *m/z* 1325.81 corresponding to Neu5Ac-Gal(Fuc)-Glc-Cer$^-$ (d18:1/18:0) sequence, $Y_{2\alpha}^-/Y_{1\gamma}^-$ at *m/z* 1179.85 corresponding to

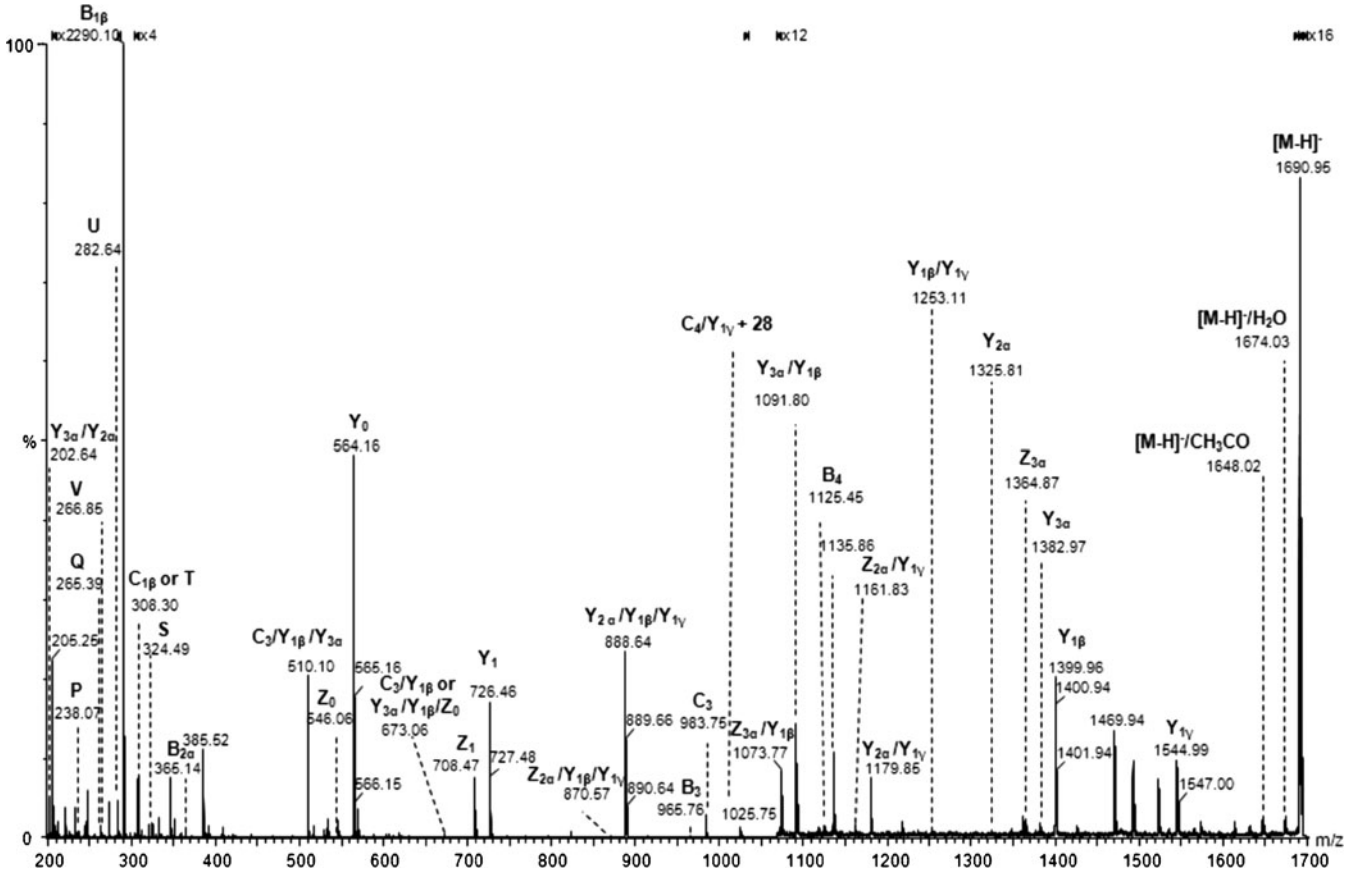

Figure 5. (–)Chip-nanoESI QTOF CID MS/MS of the singly charged ion at *m/z* 1690.95 corresponding to Fuc-GM1 (d18:1/18:0) from healthy cerebellum tissue

Neu5Ac-Gal-Glc-Cer$^-$ (d18:1/18:0) sequence together with its dehydrated counterpart $Z_{2\alpha}^-/Y_{1\gamma}^-$ at *m/z* 1161.83, $Y_{3\alpha}^-$ at *m/z* 1382.97 with the GalNAc-Gal(Fuc)(Neu5Ac)-Glc-Cer$^-$ (d18:1/18:0) sequence together with its dehydrated counterpart $Z_{3\alpha}^-$ at *m/z* 1364.87. These data give hard evidence on the presence of the GM1a structural isomer in the healthy cerebellum tissue (Figure 6).

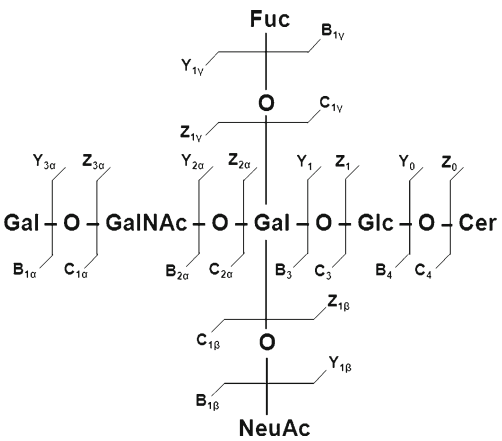

Figure 6. Fragmentation scheme by CID MS/MS of Fuc-GM1 (d18:1/18:0) ganglioside from healthy cerebellum tissue

Besides the complete characterization of the oligosaccharide sequence of the GM1 molecule and identification of the GM1a structural isomer, the MS/MS fragmentation provided data on the (d18:1/18:0) constitution of the ceramide, which is directly supported by Y_0 and Z_0 ions detected at *m/z* 564.16 and 546.06, respectively, as well as by P, Q, V, U, T, and S ions (Figure 5).

Conclusions

The present approach, combining a high performance MS method based on chip-nanoESI with HPTLC and densitometric scanning, enabled the detection and structural assignment of 125 possible distinct species expressed in brain metastasis of lung adenocarcinoma, as well as characterization of structural features of single GG components in the complex native mixture. The chromatographic and densitometric analysis indicated a several fold decrease (14×) of the total GG content in brain metastasis versus healthy human brain. GG composition of brain metastasis sample was found to be highly altered in comparison to the composition of

healthy human brain. Thus, the relative abundances of GM3 and GM2 fractions were 22.5- and 5.5-folds higher, whereas GM1, GD1b, and GT1b fractions showed 25.5-, 17.0-, and 2.1-fold lower relative abundances. These results are consistent with literature data showing that GM3 was the main ganglioside component in all metastatic tumors of human brain of various origins and that the reduced content of complex gangliosides, i.e., GM1, GD1b, GD1a, and GT1b is common for many types of transformed cells, especially for metastatic tumor cells [56–61].

Under identical experimental conditions, MS analysis of normal versus metastatic tissue sample also revealed a noticeable variation of GG expression. While brain metastasis is characterized by short ganglioside species with reduced sialic acid content and prevalence of GM type, healthy cerebellar tissue is dominated by mono- to hexasialylated structures with higher expression of GD and GT-type. The reduction in the total GG content and the altered profile of GGs in brain metastasis versus healthy control tissue could be a result of both a lower overall biosynthetic rate, due to change in expression of certain glycosyl- and sialyltransferases, and a higher turnover rate. An elevated expression of sialyltransferase I (GM3 synthase) and II (GD3 synthase) and a lower expression of galactosyltransferase II could, in part, explain the high GM3 and GD3 and the low GM1 and GD1b abundances.

MS data indicated the presence in the metastatic tissue of several unusual monosialylated species modified by fucosylation or *O*-acetylation such as Fuc-GM4, Fuc-GM3, di-*O*-Ac-GM3, and *O*-Ac-GM3. These species were previously reported as fetal brain-associated GGs, i.e., developmentally regulated antigens, which are only minor components of the normal brain [36].

GD3 (d18:1/18:0) was reported to enhance tumor cell proliferation, invasion, and metastasis in a variety of brain tumor cells, especially in glioma and neuroblastoma [62, 63]. GD3 influence tumor angiogenesis and metastasis by stimulating VEGF release from tumor cells [64], hence its structural characterization is of high biological importance. By tandem MS using CID, the oligosaccharide core of the brain metastasis-associated GD3 (d18:1/18:0) species was structurally elucidated. At the same time, a number of Cer-derived fragment ions allowed also the postulation of the lipid moiety composition.

Optimized MS/MS conditions enabled structural assessment of Fuc-GM1 (d18:1/18:0) detected in healthy cerebellum. It was found that the identified Fuc-GM1 is an atypical isomer bearing the labile Fuc residue at the inner Gal molecule together with one Neu5Ac attached at the same monosaccharide. However, the presence of the isomer with Fuc attached to the outer Gal of the carbohydrate chain can be neither excluded nor demonstrated. Because of the symmetry of the carbohydrate chain, there is no possibility for formation of diagnostic fragment ions able to unequivocally support Fuc attachment at the outer Gal. Consequently, the presence of this isomer cannot be excluded. Although the present approach allowed an unambiguous determination of Fuc localization at the inner Gal further development of NanoMate in conjunction with multiple stage fragmentation (MS^n) for discrimination between the possible (alpha1-2) and (1–6) glycosidic bond types is planned.

Finally, noteworthy to mention is that chip-nanoESI QTOF MS and CID MS/MS was able to provide compositional and structural characterization of native ganglioside mixtures from secondary brain tumors with remarkable analysis speed and sensitivity. In view of the flow rate delivered by the chip-nanoESI, which under the applied conditions was around 100 nL/min, 1 min acquisition time at a sample concentration of only 2.5 pmol/μL corresponds to 250 fmol biological extract consumption. Thus, a MS screening followed by CID MS/MS required only 500 fmols of material. For all these reasons, the bioanalytical platform demonstrated here for determination of GSL molecular markers in brain tumors has real perspectives of development into a routine, ultrafast, and sensitive method applicable to other types of cancer and molecular markers.

References

1. Sorensen, J.B., Hansen, H.H., Hansen, M., Dombernowsky, P.: Brain metastases in adenocarcinoma of the lung: frequency, risk groups, and prognosis. *J. Clin. Oncol.* **6**, 1474–1480 (1988)
2. Gow, C.H., Chien, C.R., Chang, Y.L., Chiu, Y.H., Kuo, S.H., Shih, J. Y., Chang, Y.C., Yu, C.J., Yang, C.H., Yang, P.C.: Radiotherapy in lung adenocarcinoma with brain metastases: effects of activating epidermal growth factor receptor mutations on clinical response. *Clin. Cancer Res.* **14**, 162–168 (2008)
3. Mehta, M.P., Rodrigus, P., Terhaard, C.H.J., Rao, A., Suh, J., Roa, W., Souhami, L., Bezjak, A., Leibenhaut, M., Komaki, R., Schultz, C., Timmerman, R., Curran, W., Smith, J., Phan, S.C., Miller, R.A., Renschler, M.F.: Survival and neurological outcomes in a randomized trial of motexafin gadolinium and whole-brain radiation therapy in brain metastases. *J. Clin. Oncol.* **21**, 2529–2536 (2003)
4. Ching, A.S.C., Chan, P.N., Ng, H.K., Tse, K.M., Chan, Y.L.: Isolated hemorrhagic brain metastasis from lung adenocarcinoma in a 68-year-old man. *J. K. Coll. Radiol.* **7**, 140–144 (2004)
5. Gavrilovic, I., Posner, J.: Brain metastases: epidemiology and pathophysiology. *J. Neurooncol.* **75**, 5–14 (2005)
6. Weil, R.J., Palmieri, D.C., Bronder, J.L., Stark, A.M., Steeg, P.S.: Breast cancer metastasis to the central nervous system. *Am. J. Pathol.* **167**, 913–920 (2005)
7. Ammirati, M., Cobbs, C.S., Linskey, M.E., Paleologos, N.A., Ryken, T. C., Burri, S.H., Asher, A.L., Loeffler, J.S., Robinson, P.D., Andrews, D. W., Gaspar, L.E., Kondziolka, D., McDermott, M., Mehta, M.P., Mikkelsen, T., Olson, J.J., Patchell, R.A., Kalkanis, S.N.: The role of retreatment in the management of recurrent/progressive brain metastases: a systematic review and evidence-based clinical practice guideline. *J. Neurooncol.* **96**, 85–96 (2010)
8. Gaspar, L.E., Mehta, M.P., Patchell, R.A., Burri, S.H., Robinson, P.D., Morris, R.E., Ammirati, M., Andrews, D.W., Asher, A.L., Cobbs, C.S., Kondziolka, D., Linskey, M.E., Loeffler, J.S., McDermott, M., Mikkelsen, T., Olson, J.J., Paleologos, N.A., Ryken, T.C., Kalkanis, S.N.: The role of whole brain radiation therapy in the management of newly diagnosed brain metastases: a systematic review and evidence-based clinical practice guideline. *J. Neurooncol.* **96**, 17–32 (2010)
9. Kalkanis, S.N., Kondziolka, D., Gaspar, L.E., Burri, S.H., Asher, A.L., Cobbs, C.S., Ammirati, M., Robinson, P.D., Andrews, D.W., Loeffler, J.S., McDermott, M., Mehta, M.P., Mikkelsen, T., Olson, J.J., Paleologos, N.A., Patchell, R.A., Ryken, T.C., Linskey, M.E.: The role of surgical resection in the management of newly diagnosed brain metastases: a systematic review and evidence-based clinical practice guideline. *J. Neurooncol.* **96**, 33–43 (2010)

10. Hakomori, S.: Glycosylation defining cancer malignancy: new wine in an old bottle. *Proc. Natl. Acad. Sci. U.S.A.* **99**, 10231–10233 (2002)
11. Kozbor, D.: Cancer vaccine with mimotopes of tumor-associated carbohydrated antygenes. *Immunol. Res.* **46**, 23–31 (2010)
12. Gorelik, E., Galili, U., Raz, A.: On the role of cell surface carbohydrates and their binding proteins (lectins) in tumor metastasis. *Cancer Metastasis Rev.* **20**, 245–277 (2001)
13. Colsch, B., Woods, A.S.: Localization and imaging of sialylated glycosphingolipids in brain tissue sections by MALDI mass spectrometry. *Glycobiology* **20**, 661–667 (2010)
14. Sonnino, S., Mauri, L., Chigorno, V., Prinetti, A.: Gangliosides as components of lipid membrane domains. *Glycobiology* **17**, 1R–13R (2007)
15. Rösner, H.: Developmental expression and possible roles of gangliosides in brain development. *Prog. Mol. Subcell. Biol.* **32**, 49–73 (2003)
16. Lopez, P.H., Schnaar, R.L.: Gangliosides in cell recognition and membrane protein regulation. *Curr. Opin. Struct. Biol.* **19**, 549–557 (2009)
17. El-Abbadi, M., Seyfried, T.N., Yates, A.J., Orosz, C., Lee, M.C.: Ganglioside composition and histology of a spontaneous metastatic brain tumor in the VM mouse. *Br. J. Cancer* **85**, 285–292 (2001)
18. Müthing, J., Meisen, I., Kniep, B., Haier, J., Senninger, N., Neumann, U., Langer, M., Witthohn, K., Milosević, J., Peter-Katalinić, J.: Tumor-associated CD75s gangliosides and CD75s-bearing glycoproteins with Neu5Acα2-6Galβ1-4GlcNAc residues are receptors for the anticancer drug rViscumin. *FASEB J.* **19**, 103–105 (2005)
19. Distler, U., Souady, J., Hulsewig, M., Drmic-Hofman, I., Haier, J., Denz, A., Grutzmann, R., Pilarsky, C., Senninger, N., Dreisewerd, K., Berkenkamp, S., Schmidt, M.A., Peter-Katalinic, J., Muthing, J.: Tumor-associated CD75s- and iso-CD75s-gangliosides are potential targets for adjuvant therapy in pancreatic cancer. *Mol. Cancer Ther.* **7**, 2464–2475 (2008)
20. Kohla, G., Stockfleth, E., Schauer, R.: Gangliosides with O-acetylated sialic acids in tumors of neuroectodermal origin. *Neurochem. Res.* **27**, 583–592 (2002)
21. Papini, N., Anastasia, L., Tringali, C., Croci, G., Bresciani, R., Yamaguchi, K., Miyagi, T., Preti, A., Prinetti, A., Prioni, S., Sonnino, S., Tettamanti, G., Venerando, B., Monti, E.: The plasma membrane-associated sialidase MmNEU3 modifies the ganglioside pattern of adjacent cells supporting its involvement in cell-to-cell interactions. *J. Biol. Chem.* **279**, 16989–16995 (2004)
22. Tringali, C., Lupo, B., Anastasia, L., Papini, N., Monti, E., Bresciani, R., Tettamanti, G., Venerando, B.: Expression of sialidase Neu2 in leukemic K562 cells induces apoptosis by impairing Bcr-Abl/Src kinases signaling. *J. Biol. Chem.* **282**, 14364–14372 (2007)
23. Chen, H.H., Fukumoto, S., Furukawa, K., Nakao, A., Akiyama, S., Urano, T., Furukawa, K.: Suppression of lung metastasis of mouse Lewis lung cancer p29 with transfection of the ganglioside Gm2/Gd2 synthase gene. *Int. J. Cancer* **103**, 169–176 (2003)
24. Noguchi, M., Suzuki, T., Kabayama, K., Takahashi, H., Chiba, H., Shiratori, M., Abe, S., Watanabe, A., Satoh, M., Hasegawa, T., Tagami, S., Ishii, A., Saitoh, M., Kaneko, M., Iseki, K., Igarashi, Y., Inokuchi, J. I.: GM3 synthase gene is a novel biomarker for histologic classification and drug sensitivity against epidermal growth factor receptor tyrosine kinase inhibitors in non-small-cell lung cancer. *Cancer Sci.* **98**, 1625–1632 (2007)
25. Uemura, S., Kabayama, K., Noguchi, M., Igarashi, Y., Inokuchi, J.I.: Sialylation and sulfation of lactosylceramide distinctly regulate anchorage-independent growth, apoptosis, and gene expression in3LL Lewis lung carcinoma cells. *Glycobiology* **13**, 207–216 (2003)
26. Zhang, Q., Furukawa, K., Chen, H.H., Sakakibara, T., Urano, T., Furukawa, K.: Metastatic potential of mouse Lewis lung cancer cells is regulated via ganglioside GM1 by modulating the matrix metalloprotease-9 localization in lipid rafts. *J. Biol. Chem.* **281**, 18145–18155 (2006)
27. Tokuda, N., Zhang, Q., Yoshida, S., Kusunoki, S., Urano, T., Furukawa, K., Furukawa, K.: Genetic mechanisms for the synthesis of fucosyl GM1 in small cell lung cancer cell lines. *Glycobiology* **16**, 916–925 (2006)
28. Nagorny, P., Kim, W.H., Wan, Q., Lee, D., Danishefsky, S.J.: On the emerging role of chemistry in the fashioning of biologics: synthesis of a bidomainal fucosyl GM1-based vaccine for the treatment of small cell lung cancer. *J. Org. Chem.* **74**, 5157–5162 (2009)
29. Diaz, Y., Gonzalez, A., Lopez, A., Perez, R., Vazquez, A.M., Montero, E.: Anti-ganglioside anti-idiotypic monoclonal antibody-based cancer vaccine induces apoptosis and antiangiogenic effect in a metastatic lung carcinoma. *Cancer Immunol. Immunother.* **58**, 1117–1128 (2009)
30. Fredman, P., Brezicka, T., Holmgren, J., Lindholm, L., Nilsson, O., Svennerholm, L.: Binding specificity of monoclonal antibodies to ganglioside Fuc-GM. *Biochim. Biophys. Acta* **75**, 316–323 (1986)
31. Muthing, J., Distler, U.: Advances on the compositional analysis of glycosphingolipids combining thin-layer chromatography with mass spectrometry. *Mass Spectrom. Rev.* **29**, 425–479 (2010)
32. Ting, Y.S., Shaffer, S.A., Jones, J.W., Ng, W.V., Ernst, R.K., Goodlett, D.R.: Automated lipid A structure assignemnt from hierachical tandem mass spectrometry data. *J. Am. Soc. Mass Spectrom.* **22**, 856–866 (2011)
33. Jones, J.W., Cohen, I.E., Turecek, F., Goodlett, D.R., Ernst, R.K.: Comprehensive structure characterization of lipid A extracted from Yersinia pestis for determination of its phosphorilation configuration. *J. Am. Soc. Mass Spectrom.* **21**, 785–799 (2010)
34. Zamfir, A.D., Flangea, C., Altmann, F., Rizzi, A.: Glycosylation analysis of proteins, proteoglycans, and glycolipids using capillary electrophoresis and mass spectrometry. *Adv. Chromatogr.* **49**, 135–194 (2011)
35. Vukelić, Z., Kalanj-Bognar, S., Froesch, M., Bîndila, L., Radić, B., Allen, M., Peter-Katalinić, J., Zamfir, A.D.: Human gliosarcoma-associated ganglioside composition is complex and distinctive as evidenced by high-performance mass spectrometric determination and structural characterization. *Glycobiology* **17**, 504–515 (2007)
36. Zamfir, A., Vukelić, Z., Bindila, L., Peter-Katalinic, J., Almeida, R., Sterling, A., Allen, M.: Fully-automated chip-based nanoelectrospray tandem mass spectrometry of gangliosides from human cerebellum. *J. Am. Soc. Mass. Spectrom.* **15**, 1649–1657 (2004)
37. Vukelić, Z., Zarei, M., Peter-Katalinić, J., Zamfir, A.D.: Analysis of human hippocampus gangliosides by fully-automated chip-based nanoelectrospray tandem mass spectrometry. *J. Chromatogr. A* **1130**, 238–245 (2006)
38. Serb, A., Schiopu, C., Flangea, C., Vukelić, Ž., Şişu, E., Zagrean, L., Zamfir, A.D.: High-throughput analysis of gangliosides in defined regions of fetal brain by fully automated chip-based nanoelectrospray ionization multistage mass spectrometry. *Eur. J. Mass Spectrom.* **15**, 541–553 (2009)
39. Serb, A., Schiopu, C., Flangea, C., Sisu, E., Zamfir, A.D.: Top-down glycolipidomics: fragmentation analysis of ganglioside oligosaccharide core and ceramide moiety by chip-nanoelectrospray collision-induced dissociation MS(2)-MS(6). *J. Mass Spectrom.* **44**, 1434–1442 (2009)
40. Schiopu, C., Flangea, C., Capitan, F., Serb, A., Vukelić, Ž., Kalanj-Bognar, S., Sisu, E., Przybylski, M., Zamfir, A.D.: Determination of ganglioside composition and structure in human brain hemangioma by chip-based nanoelectrospray ionisation tandem mass spectrometry. *Anal. Bioanal. Chem.* **395**, 2465–2477 (2009)
41. Almeida, R., Mosoarca, C., Chirita, M., Udrescu, V., Dinca, N., Vukelić, Z., Allen, M., Zamfir, A.D.: Coupling of fully automated chip-based electrospray ionization to high-capacity ion trap mass spectrometer for ganglioside analysis. *Anal. Biochem.* **378**, 43–52 (2008)
42. Dall'Olio, F.: The sialyl-alpha2,6-lactosaminyl-structure: biosynthesis and functional role. *Glycoconj J* **17**, 669–676 (2000)
43. Svennerholm, L., Fredman, P.: A procedure for the quantitative isolation of brain gangliosides. *Biochim. Biophys. Acta* **617**, 97–109 (1980)
44. Vukelić, Ž., Metelmann, W., Müthing, J., Kos, M., Peter-Katalinić, J.: Anencephaly: structural characterization of gangliosides in defined brain regions. *Biol. Chem.* **382**, 259–274 (2001)
45. Svennerholm, L.: Quantitative estimation of sialic acids II. A colorimetric resorcinol- hydrochloric acid method. *Biochim. Biophys. Acta* **24**, 104–111 (1957)
46. Miettinen, T., Takki-Luukkainen, I.T.: Use of buthylacetate in determination of sialic acid. *Acta Chem. Scand.* **13**, 656–658 (1959)
47. Trbojević-Čepe, M., Kračun, I.: Determination of gangliosides in human cerebrospinal fluid by high-performance thin-layer chromatography and direct densitometry. *J. Clin. Chem. Clin. Biochem.* **8**, 863–872 (1990)
48. Domon, B., Costello, C.E.: A systematic nomenclature for carbohydrate fragmentation in FAB-MS/MS spectra of glycoconjugates. *Glycoconj. J.* **5**, 397–409 (1988)
49. Ann, Q., Adams, J.: Structure determination of ceramides and neutral glycosphingolipids by collisional activation of $[M+Li]^+$ ions. *J. Am. Soc. Mass Spectrom.* **3**, 260–266 (1992)

50. Nilsson, O., Svennerholm, L.: Characterization and quantitative determination of gangliosides and neutral glycosphingolipids in human liver. *J. Lipid Res.* **23**, 327–334 (1982)
51. Keranen, A.: Gangliosides of the human gastrointestinal mucosa. *Biochim. Biophys. Acta* **409**, 320–328 (1975)
52. Narasimhan, R., Murray, R.K.: Neutral glycosphingolipids and gangliosides of human lung and lung tumours. *Biochem J.* **179**, 199–211 (1979)
53. Metelmann, W., Vukelić, Ž., Peter-Katalinić, J.: Nano-electrospray ionization time-of-flight mass spectrometry of gangliosides from human brain tissue. *J. Mass Spectrom.* **36**, 21–29 (2001)
54. Vukelić, Z., Zamfir, A.D., Bindila, L., Froesch, M., Peter-Katalinić, J., Usuki, S., Yu, R.K.: Screening and sequencing of complex sialylated and sulfated glycosphingolipid mixtures by negative ion electro-spray Fourier transform ion cyclotron resonance mass spectrometry. *J. Am. Soc. Mass Spectrom.* **16**, 571–580 (2005)
55. Iwamori, M., Domino, S.E.: Tissue-specific loss of fucosylated glycolipids in mice with targeted deletion of alpha (1,2)fucosyltransferase genes. *Biochem. J.* **380**, 75–81 (2004)
56. Hamasaki, H., Aoyagi, M., Kasama, T., Handa, S., Hirakawa, K., Taki, T.: GT1b in human metastatic brain tumors: GT1b as a brain metastasis-associated ganglioside. *Biochim. Biophys. Acta* **1437**, 93–99 (1999)
57. Brady, R.O., Fishman, P.H.: Biosynthesis of glycolipids in virus-transformed cells. *Biochim. Biophys. Acta* **355**, 121–148 (1974)
58. Hakomori, S.: Structures and organization of cell surface glycolipids dependency on cell growth and malignant transformation. *Biochim. Biophys. Acta* **417**, 56–89 (1975)
59. Mugnai, G., Coppini, R., Tombaccini, D., Fallani, A., Ruggieri, S.: Neutral glycolipids and gangliosides of concanavalin A-selected SV3T3 revertant cells and of normal and SV40-transformed Balb/c 3 T3 cells. *Biochem. J.* **193**, 1025–1028 (1981)
60. Calorini, L., Fallani, A., Tombaccini, D., Barletta, E., Mugnai, G., Di Renzo, M.F., Comoglio, P.M., Ruggieri, S.: Lipid characteristics of RSV-transformed Balb/c 3 T3 cell lines with different spontaneous metastatic potentials. *Lipids* **24**, 685–690 (1989)
61. Ruggieri, S., Mugnai, G., Mannini, A., Calorini, L., Fallani, A., Barletta, E., Mannori, G., Cecconi, O.: Lipid characteristics in metastatic cells. *Clin. Exp. Metast.* **17**, 271–276 (1999)
62. Mukherjee, P., Faber, A.C., Shelton, L.M., Baek, R.C., Chiles, T.C., Seyfried, T.N.: Thematic review series: sphingolipids. Ganglioside GM3 suppresses the proangiogenic effects of vascular endothelial growth factor and ganglioside GD1a. *J. Lipid Res.* **49**, 929–938 (2008)
63. Petro, K.A., Schengrund, C.L.: Membrane raft disruption promotes axonogenesis in N2a neuroblastoma cells. *Neurochem. Res.* **34**, 29–37 (2009)
64. Koochekpour, S., Merzak, A., Pilkington, G.J.: Vascular endothelial growth factor production is stimulated by gangliosides and TGF-β isoforms in human glioma cells in vitro. *Cancer Lett.* **102**, 209–215 (1996)